Physica D 446 (2023) 133667

Contents lists available at ScienceDirect

Physica D

journal homepage: www.elsevier.com/locate/physd

Nested mixed-mode oscillations, Part III: Comparison of bifurcation structures between a driven Bonhoeffer–van der Pol oscillator and Nagumo–Sato piecewise-linear discontinuous one-dimensional map

Naohiko Inaba [a], Tadashi Tsubone [b], Hidetaka Ito [c,*], Hideaki Okazaki [a], Tetsuya Yoshinaga [d]

[a] Graduate School of Electrical and Information Engineering, Shonan Institute of Technology, Fujisawa 251–8511, Japan
[b] Department of Electrical, Electronics and Information Engineering, Nagaoka University of Technology, Nagaoka 940–2188, Japan
[c] Department of Electrical, Electronic and Information Engineering, Kansai University, Suita 564–8680, Japan
[d] Institute of Health Biosciences, The University of Tokushima, Tokushima 770–8509, Japan

ARTICLE INFO

Article history:
Received 1 August 2022
Received in revised form 7 January 2023
Accepted 21 January 2023
Available online 26 January 2023
Communicated by T. Insperger

Keywords:
Nested mixed-mode oscillations
Mixed-mode oscillation-incrementing bifurcations
Driven Bonhoeffer–van der Pol oscillator
Nagumo–Sato map
Nested period-adding bifurcations

ABSTRACT

In our previous studies (Inaba and Kousaka, (2020); Inaba and Tsubone, (2020)), we discovered bifurcation structures represented by nested mixed-mode oscillations (MMOs) generated by a driven Bonhoeffer–van der Pol (BVP) oscillator. BVP oscillators are equivalent to FitzHugh–Nagumo models and have been a subject of intense research for the last six decades. In this study, we consider the case in which the diode included in a driven BVP oscillator is assumed to operate as an ideal switch. In this case, Poincaré return maps can be rigorously constructed one-dimensionally, which consist of two downward convex branches. We also consider the Poincaré return map that is approximated as a two-segment piecewise-linear discontinuous one-dimensional map. Such a piecewise-linear map was proposed by Nagumo and Sato and generates nested period-adding bifurcations. We show that un-nested, singly, and doubly nested MMO-incrementing bifurcations generated by the driven BVP oscillator coincide with one of the possible un-nested, singly, and doubly nested period-adding bifurcations, respectively, generated with the Nagumo–Sato map.

1. Introduction

Canard explosions were one of the major discoveries in the 1980s [1–7], and mixed-mode oscillations (MMOs) are a phenomenon that was observed in chemical and electro-chemical experiments [8–12] during approximately the same period. A basic MMOs pattern comprises L-large oscillations and s-small peaks and are denoted by the notation L^s. Ever since recent numerical and theoretical analyses for MMOs [12–16] clarified that they can be generated in extended slow-fast and multiple time-scale dynamics that can generate canard explosions [1–7], MMOs have been the subject of intense research in many fields [17–36]. They can be numerically observed in various dynamics such as noise-induced oscillators near relaxation oscillations or canards [37–39], coupled and forced electric circuits [26–28,40–42], extended three-variable oscillators [22–24,29,43], fractional derivative dynamics [44], and medical systems [45].

Maselko et al. [10] and Albahadily et al. [11] demonstrated that MMOs occur in accordance with the rules of Farey arithmetic. Maselko [10] introduced parents–daughter processes to explain the concatenation events of two MMOs. If we denote two basic MMO sequences using $L_1^{s_1}$ and $L_2^{s_2}$ notations, they can be parents and generate a daughter $L_1^{s_1}L_2^{s_2}$ between the $L_1^{s_1}$- and $L_2^{s_2}$-generating regions, which satisfies Farey arithmetic because the firing number $L/(L+s)$ for $L_1^{s_1}L_2^{s_2}$ is $(L_1+L_2)/\{(L_1+L_2)+(s_1+s_2)\}$. The parents–daughter processes occur sequentially, and MMO waveforms $L_1^{s_1}(L_2^{s_2})^m$ emerge between the $L_1^{s_1}(L_2^{s_2})^{m-1}$- and $L_2^{s_2}$-generating regions for successive $m\,(\geq 1)$.

Shimizu et al. [26] discovered the simplest parents–daughter processes $1^2(1^3)^m$ or, more precisely, $[1^2, 1^3 \times m]_{m+1}$ in a driven BVP oscillator, which indicates that 1^2 is followed by 1^3 repeated m times in the $(m+1)$ period of the forcing term per MMO sequence. They called the resulting MMO-adding processes MMO-incrementing bifurcations (MMOIBs) [26]. Such processes increment sequentially and terminate until the whole sequences are replaced by successive 1^3s. MMOIBs are well-known parents–daughter processes that were frequently observed in autonomous

* Corresponding author.
E-mail address: h.ito@kansai-u.ac.jp (H. Ito).

https://doi.org/10.1016/j.physd.2023.133667

[22,23,46,47] and nonautonomous ordinary differential equations (ODEs) [28,29,48]; thus, we call them zero-degree (un-nested) MMOIBs, which are generated between two adjacent simple MMOs. Un-nested MMOIBs occur in a fashion similar to period-adding bifurcations generated by circle maps [22,23,28,29,47,49,50].

The fundamental mechanism causing simple MMOs has been analyzed theoretically by several researchers [15,17–19,30,31,34]. However, at present, there are many things that are not clear about MMOIBs [22,23,26–29,43] even numerically. Un-nested MMOIBs have generated intensive research attention and have been extensively studied numerically in both autonomous [13,16,22,23,29,43,47] and nonautonomous [20,21,26,27,50,51] ODEs.

In previous works [48,51–54], we discovered bifurcation structures of nested MMOs generated by a driven BVP oscillator. It is known that BVP oscillators are equivalent to FitzHugh–Nagumo dynamics [55,56] and have been studied extensively. They can be nested at least twice [51,52,54]. The generation patterns of nested MMOs are as follows. Let two adjacent simple MMOs be denoted by $1^s \equiv A_0$ and $1^{s+1} \equiv B_0$. The number of large oscillations $L = 1$ could be fundamental in extended and forced BVP dynamics [46–48,51–53]. Then, un-nested MMOIBs generate MMO sequences denoted by $[A_0, B_0 \times m]$ for successive m ($\geq$ 1) between the $[A_0, B_0 \times (m-1)]$- and B_0-generating regions, where $[A_0, B_0 \times m]$ indicates that A_0 is followed by B_0 repeated m times. In this notation, $[A_0, B_0 \times 0] = A_0$. Next, let two adjacent un-nested MMOIB-generated MMOs be denoted by $[A_0, B_0 \times m] \equiv A_1$ and $[A_0, B_0 \times (m+1)] \equiv B_1$, where m is one of the integer values. We then call the following more highly nested MMOIB-generated MMOs that occur between two adjacent complex MMOs (i.e., A_1 and B_1) nested MMOs, which exhibit nested trajectories on Poincaré return maps. To the best of our knowledge, nested MMOs can be observed in nonautonomous ODEs [51,52,54] and not in autonomous ODEs [22,23,47]. Singly nested MMOIBs generate MMO sequences denoted by $[A_1, B_1 \times p]$ for successive p ($\geq$ 1) between the $[A_1, B_1 \times (p-1)]$- and B_1-generating regions. Similarly, $[A_1, B_1 \times p]$ indicates that A_1 is followed by B_1 repeated p times. The nested MMOIBs occur at least twice. Let two adjacent singly nested MMOIB-generated MMOs be denoted by $[A_1, B_1 \times p] \equiv A_2$ and $[A_1, B_1 \times (p+1)] \equiv B_2$, where p is one of the integer values. Then, doubly nested MMOIBs generate MMO sequences denoted by $[A_2, B_2 \times q]$ sequentially between the $[A_2, B_2 \times (q-1)]$- and B_2-generating regions. Similarly, $[A_2, B_2 \times q]$ indicates that A_2 is followed by B_2 repeated q times. However, our previous results [48,51–53] have focused on the BVP oscillator in a rather complex case with the bistability of a stable focus and a relaxation oscillation in the absence of perturbation that exist as a result of a subcritical Hopf bifurcation. For clarity, we summarize the definition of un-nested and nested MMOs in Table 1.

In this study, we focus on the slow-fast BVP oscillator in a simpler case where the dynamics have a small amplitude oscillation (canard without a head) as a result of a supercritical Hopf bifurcation in the absence of perturbations [54]. Furthermore, to analyze un-nested, singly and doubly nested MMOIB-generated MMOs, we consider an idealized case where the diode contained in the oscillator is approximated as an ON–OFF switch [57–59]. This idealization of the diode corresponds to a degenerated case where one of the parameters tends to infinity and the governing equation is derived as a constrained equation. In this case, one-dimensional (1D) Poincaré return maps can be constructed from the oscillator. It has been clarified that MMOIBs occur on the two downward convex branches in the invariant interval on the return map. In addition, numerical results have been verified in circuit experiments.

To investigate how nested MMOIB-generated MMOs emerge, we consider a piecewise-linear discontinuous approximation for

Table 1
Definition of un-nested and nested MMOs.

Definition	Pattern
un-nested MMOIB-generated MMOs	$[A_0, B_0 \times m]$ for successive m (≥ 1), where $A_0 = 1^s$ and $B_0 = 1^{s+1}$
singly nested MMOIB-generated MMOs	$[A_1, B_1 \times p]$ for successive p (≥ 1), where $A_1 = [A_0, B_0 \times m]$ and $B_1 = [A_0, B_0 \times (m+1)]$
doubly nested MMOIB-generated MMOs	$[A_2, B_2 \times q]$ for successive q (≥ 1), where $A_2 = [A_1, B_1 \times p]$ and $B_2 = [A_1, B_1 \times (p+1)]$

1D Poincaré return maps. Such a piecewise-linear discontinuous 1D map has been analyzed by Nagumo and Sato, Hata, Yoshida, Doi, and Leonov [60–68]. We call the piecewise-linear discontinuous 1D map a Nagumo–Sato map. The contents of the Nagumo–Sato map discussed by Leonov are briefly described in Ref. [69] by Mira. In the Nagumo–Sato map, period-adding bifurcations are nested infinitely many times, and a devil's staircase emerges [60,69]. There are large differences between the driven BVP oscillator and the Nagumo–Sato map, however; mirror sequences always appear in the Nagumo–Sato map, whereas mirror sequences do not emerge in the driven BVP oscillator because both branches in the Poincaré return map are downward convex in the BVP oscillator. For example, in the Nagumo–Sato map, period-adding bifurcations occur when either of the two branches approaches a diagonal line, whereas the lower branch of the Poincaré return map cannot be tangential to the diagonal line in the BVP oscillator because the branch is downward convex. Thus, among the possible solutions in the Nagumo–Sato map, only one solution with the same symbol appears as an attractor in the driven BVP oscillator. Namely, the lower and upper branches in the Nagumo–Sato map correspond to 1 and 0, respectively, and 0 and 1 correspond to A_0 and B_0, respectively. Then, "$0111\cdots$" and "$1000\cdots$" appear in the Nagumo–Sato map, whereas only "$0111\cdots$" can appear in the driven BVP oscillator, i.e., we conclude that the Farey trees in the BVP oscillator are asymmetric. Since the period-adding bifurcations can be nested as many times as desired in the Nagumo–Sato map, these results suggest that more deeply nested MMOs could exist in the driven BVP oscillator.

2. Circuit setup of constrained BVP oscillator with diode under weak periodic perturbations

Fig. 1 shows a circuit diagram for a driven BVP oscillator with the idealized diode discussed in Ref. [50–52]. In the figure, L, C, R, E_0, and $E_1 \sin\omega_1 t$ are an inductor, capacitor, linear resistor, DC bias, and sinusoidal voltage source. In addition, G_1 and G_2 are nonlinear conductors, where G_1 has third-order nonlinear voltage–current characteristics, i.e., $G_1(v) = -g_1 v + g_3 v^3$, and G_2 represents a piecewise linear diode:

$$G_2(v) = \begin{cases} 0, & v < V, \\ g(v - V), & v \geq V, \end{cases} \tag{1}$$

where $g_1, g_3, g, V > 0$. g is the ON conductance of the diode and is usually large. Since $G_0(v) = I_1 + I_2$ (see Fig. 1), the current flowing through the capacitor in the reverse direction of v is Cdv/dt, and the voltage generated across the inductor in the reverse direction of i is Ldi/dt, the governing equation is written by the following system of two nonautonomous ODEs.

$$\begin{cases} C\dfrac{dv}{dt} &= i - G_0(v), \\ L\dfrac{di}{dt} &= -v - Ri + E_0 + E_1 \sin\omega_1 t, \end{cases} \tag{2}$$

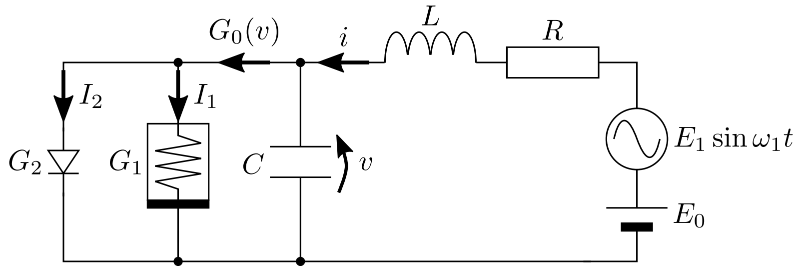

Fig. 1. Driven BVP circuit with idealized diode.

where $\omega_1 = 2\pi f$ (f is the frequency of the forcing term), and

$$G_0(v) = \begin{cases} I_1(v) + I_2(v) = -g_1 v + g_3 v^3, & v < V, \\ I_1(v) + I_2(v) = -g_1 v + g_3 v^3 + g(v - V), & v \geq V. \end{cases} \quad (3)$$

In Eq. (2), C is assumed to be small. Therefore, the governing equation then represents slow-fast dynamics, where v and i are fast and slow variables, respectively. (Note that we use the notation L to express the number of large excursions in MMOs, but these two cannot be confused.)

Using the following rescaling,

$$\tau = \frac{t}{Lg_1}, \varepsilon = \frac{C}{g_1^2 L}, k_1 = g_1 R, \omega = Lg_1\omega_1,$$
$$B_0 = \sqrt{\frac{g_3}{g_1}} E_0, B_1 = \sqrt{\frac{g_3}{g_1}} E_1, x = \sqrt{\frac{g_3}{g_1}} v, \quad (4)$$
$$y = \sqrt{\frac{g_3}{g_1^3}} i, u = \frac{g}{g_1}, \alpha = \sqrt{\frac{g_3}{g_1}} V,$$

(In this study, we also used the notation B_0 as a simple MMO pattern 1^{s+1}, but there should be no confusion.) Eq. (2) is transformed to the following equation.

$$\begin{cases} \varepsilon \dot{x} &= y - g_0(x), \\ \dot{y} &= -x - k_1 y + B_0 + B_1 \sin\omega\tau, \end{cases} \quad (5)$$

where ε is a small parameter, where the dot over the variables denotes the first-order derivative with respect to time τ and g_0 is written by

$$g_0(x) = \begin{cases} -x + x^3, & x < \alpha, \\ -x + x^3 + u(x - \alpha), & x \geq \alpha. \end{cases} \quad (6)$$

Here, we consider the limit where u tends to infinity. The voltage–current characteristics of $g_0(x)$ that includes an ON–OFF diode are shown in Fig. 2. In this idealized case, x is constrained to a constant α, and the dynamics are approximated by the following constrained ODEs:

1. diode OFF:
$$\begin{cases} \varepsilon\dot{x} = y - g_0(x), \\ \dot{y} = -x - k_1 y + B_0 + B_1 \sin\omega\tau, \end{cases}$$
$$\Downarrow x = \alpha \quad \Uparrow y = -\alpha + \alpha^3 (= g_0(\alpha)), \quad (7)$$
2. diode ON:
$$\begin{cases} x = \alpha, \\ \dot{y} = -\alpha - k_1 y + B_0 + B_1 \sin\omega\tau. \end{cases}$$

The symbols $\Downarrow$ and $\Uparrow$ represent the transition conditions. Since x is a constant when the diode is in the ON state, the lower pair of equations can be expressed by a one-variable nonautonomous equation. The transition $\Uparrow$ occurs when $y = -\alpha + \alpha^3 (= g_0(\alpha))$ because $\dot{x} = 0$ (x is constant when the diode is in the ON state), and therefore, the current flowing through the nonlinear conductor satisfies the equation $g_0(\alpha) = y$ at the transition from the ON state to the OFF state.

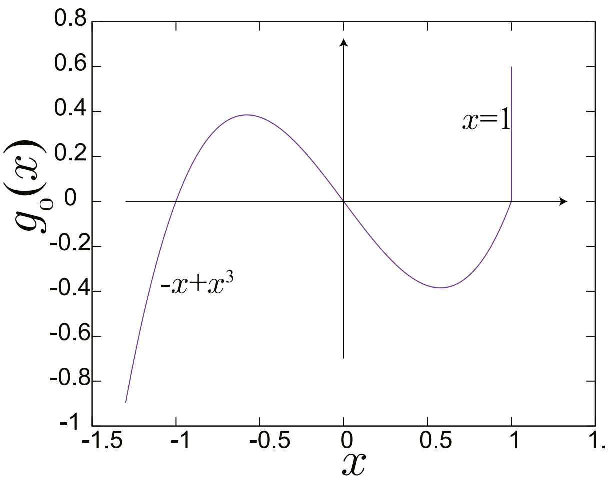

Fig. 2. Voltage–current characteristics of nonlinear conductance $g_0(x)$ that contains ON–OFF diode with complete saturation ($\alpha = 1$).

Such an idealization method using constrained ODEs was proposed by Inaba et al. [57–59] to precisely analyze chaos and torus breakdown generated by extended and driven van der Pol oscillators with a diode in the 1980s–1990s. These constrained dynamics with an idealized diode have similar characteristics to stick–slip mechanical oscillators with dry friction [70–72]. Inaba et al. [47,49–52] succeeded in explaining successive MMOIB-generated MMOs precisely generated by extended and driven BVP oscillators using 1D Poincaré return maps.

In the following discussion, we set $\alpha = 1$ (see Figs. 2 and 3), $\varepsilon = 0.1$, $k_1 = 0.2$, $B_0 = 0.49$, and $B_1 = 0.008$, and we select ω as the bifurcation parameter.

A structure on the x–y plane in the absence of perturbation is shown in Fig. 3. In the case of $B_1 = 0$, a small amplitude oscillation (canard without a head) exists as a result of a supercritical Hopf bifurcation [54]. By adding weak periodic perturbations, various MMOs emerge.

In Ref. [54], we focused on nested MMOs between the 1^3- and 1^4-generating regions, which occur in the BVP oscillator that has a canard without a head in the absence of perturbations, where the constrained ODEs with an idealized diode was not considered. In this study, we do so between the 1^2- and 1^3-generating regions and adopt the idealization of a diode. If this idealization is used, Poincaré return maps can be constructed one-dimensionally. Figs. 4(a.1) and (e) show time series waveforms of simple 1^2 and 1^3 MMOs. Fig. 4(a.2) shows the projection of Fig. 4(a.1) onto the x–y plane. From this figure, we can see

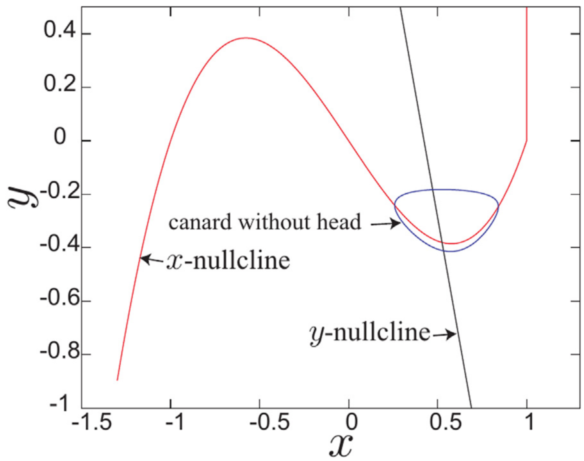

Fig. 3. Structure on x–y plane in absence of perturbation ($\alpha = 1, \varepsilon = 0.1, k_1 = 0.2, B_0 = 0.49$, and $B_1 = 0$). x-nullcline: red, y-nullcline: black, and canard oscillation without head: blue.

that the attractor is constrained onto $x = \alpha(= 1)$. Figs. 4(b)–(d) show time series waveforms of un-nested MMOIB-generated $[1^2, 1^3 \times m]_{m+1}$ MMOs for $m = 1$–3, respectively.

3. One-parameter bifurcation diagrams and un-nested, singly and doubly nested MMOs in driven BVP oscillator

To analyze MMO bifurcations precisely, Poincaré return maps are introduced. Since the equation for the ON state is given by 1D nonautonomous ODEs, 1D Poincaré return maps can be exactly defined as follows.

To define the 1D Poincaré return maps, we define a line Σ_1 and half plane π_1 as

$$\begin{aligned} \pi_1 &= \{(\tau, x, y) | x - \alpha = 0, y - g_0(x) < 0 \ (\dot{x} < 0) \}, \\ \Sigma_1 &= \{(\tau, x, y) | x - \alpha = 0, y - g_0(x) = 0 \}, \end{aligned} \tag{8}$$

(see Fig. 5). π_1 is a half plane where the diode is in the ON state, and Σ_1 is a line at which the transition $\Uparrow$ from the ON state to the OFF state occurs.

Let us consider a solution where the initial condition is situated on line Σ_1 at $(\tau, x, y) = (\tau_0, 1, -\alpha + \alpha^3(= g_0(\alpha)))$ as shown in Fig. 5. The solution leaving line Σ_1 enters the diode-OFF region, strikes π_1 at a point marked P, and strikes Σ_1 again at $(\tau, x, y) = (\tau_1, 1, -\alpha + \alpha^3(= g_0(\alpha)))$. Therefore, we can define the 1D Poincaré return map T that transforms τ_0 to τ_1 as

$$T : \Sigma_1 \to \Sigma_1, \theta_0 \mapsto \theta_1, \tag{9}$$

where $\theta_0 = \omega\tau_0/2\pi$, and $\theta_1 = \omega\tau_1/2\pi \mod 1$.

Even if the diode is not assumed to operate as an ideal switch, similar return maps, which we refer to as first return plots [51,54], can be defined in a similar manner. Such first return plots are only approximately defined in one-dimensional space. We emphasize that the diode idealization permits the exact construction of 1D Poincaré return maps.

Fig. 6 shows a global view of a one-parameter bifurcation diagram between the $1^2 \equiv A_0$- and $1^3 \equiv B_0$-generating regions. Un-nested MMOIB-generated $[A_0, B_0 \times m] = [1^2, 1^3 \times m]_{m+1}$ MMOs can be observed sequentially for successive m, which indicate that A_0 is followed by B_0 repeated m times. Note that the subscript indicates the number of periods of the forcing term per MMO, and it equals the number of large oscillations.

Figs. 7(a)–(d) show 1D Poincaré return maps and the corresponding trajectories for $[A_0, B_0 \times m] = [1^2, 1^3 \times m]_{m+1}$ with $m = 1, 2, 3$, and 10, respectively. Since MMOIBs occur sequentially until the 1^3 branch is tangential to the diagonal line, they could occur as many times as we track. We call this tangent point an MMO increment–terminating tangent bifurcation [51,52]. The parameter values at the tangent point can be derived by solving the following simultaneous equations numerically:

$$\begin{aligned} &T(\theta, \omega) = \theta, \\ &\frac{\partial}{\partial\theta} T(\theta, \omega) = 1. \end{aligned} \tag{10}$$

The return map T at the tangent point is shown in Fig. 8. Note that since the branch generating 1^2 in the invariant interval of the Poincaré return map cannot be tangential to the diagonal line, the dynamics can generate asymmetric Farey trees.

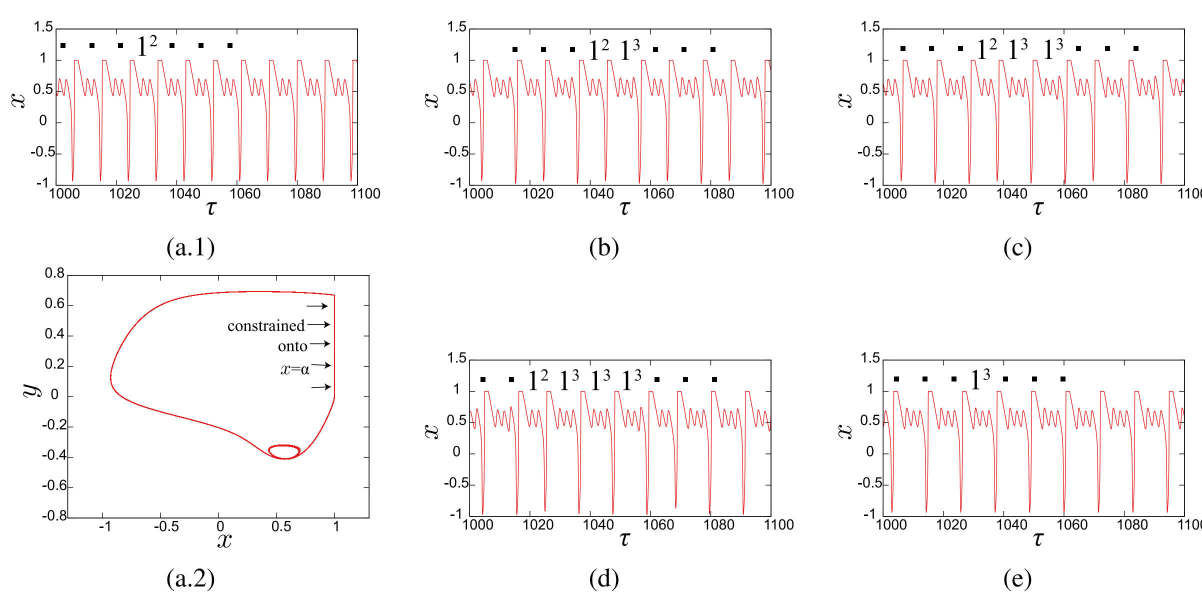

Fig. 4. Time series waveforms and attractor, showing (a.1) 1^2 with $\omega = 0.68$, (a.2) projection of attractor of (a.1) onto x–y plane, (b) $[1^2, 1^3 \times 1]_2$ with $\omega = 0.612$, (c) $[1^2, 1^3 \times 2]_3$ with $\omega = 0.592$, (d) $[1^2, 1^3 \times 3]_4$ with $\omega = 0.581$, and (e) 1^3 with $\omega = 0.55$.

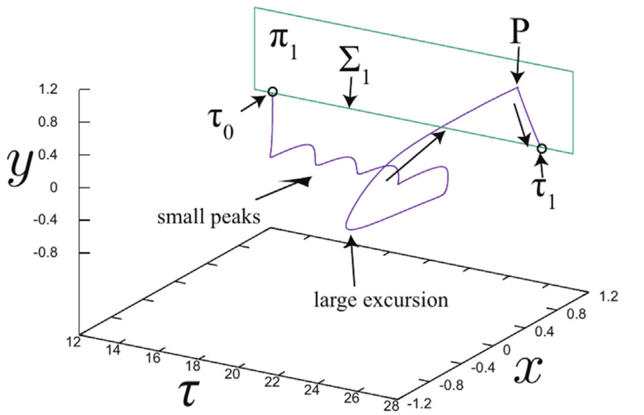

Fig. 5. Definition of 1D Poincaré return maps for constrained circuit with idealized diode represented by Eq. (7).

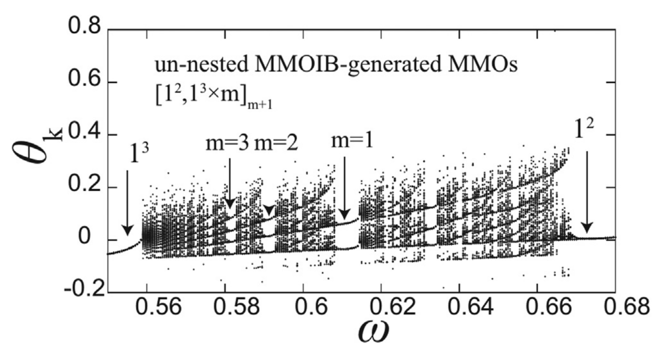

Fig. 6. Global view of one-parameter bifurcation diagram between the 1^2- and 1^3-generating regions.

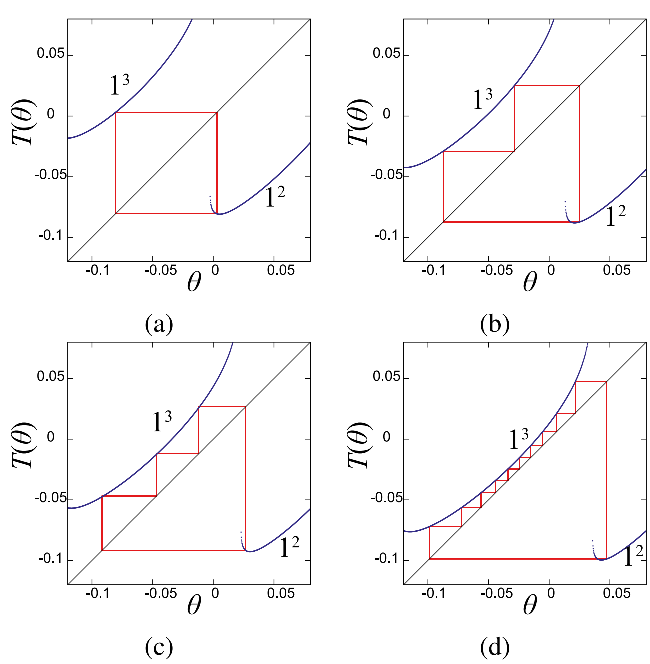

Fig. 7. 1D Poincaré return maps and corresponding trajectories for un-nested MMOIB-generated MMOs $[1^2, 1^3 \times m]_{m+1}$, showing (a) $m = 1$ with $\omega = 0.612$, (b) $m = 2$ with $\omega = 0.592$, (c) $m = 3$ with $\omega = 0.581$, and (d) $m = 10$ with $\omega = 0.5649$.

Next, we focus on the parameter interval between the $[1^2, 1^3 \times 1]_2 \equiv A_1$- and $[1^2, 1^3 \times 2]_3 \equiv B_1$-generating regions. Fig. 9 shows a magnified one-parameter bifurcation diagram. Self-similar structures can be observed, i.e., between the A_1- and B_1-generating regions, $[A_1, B_1 \times p] = [[1^2, 1^3 \times 1]_2, [1^2, 1^3 \times 2]_3 \times p]_{3p+2}$ can be observed sequentially for successive p, which exhibit singly nested MMOs. As a consequence, the driven BVP dynamics can generate very complex time series waveforms, as shown in Ref. [54], which could not be easily distinguished only by observing the MMO waveforms alone [51,52,54].

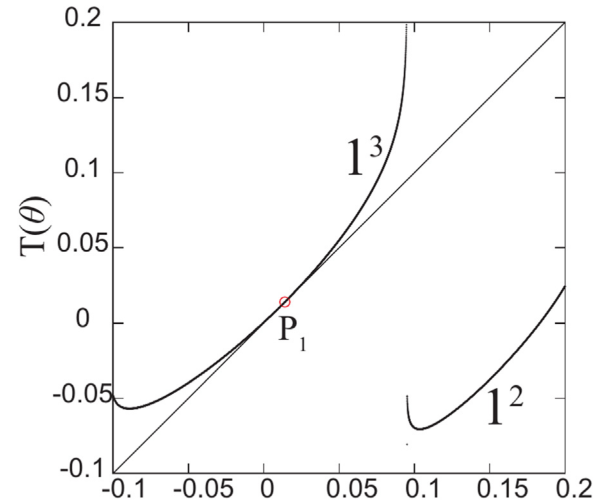

Fig. 8. T at MMO incrementing–terminating bifurcation point for $[A_1, B_1 \times m]$ with $m \to \infty$ for $\omega = 0.5587274$.

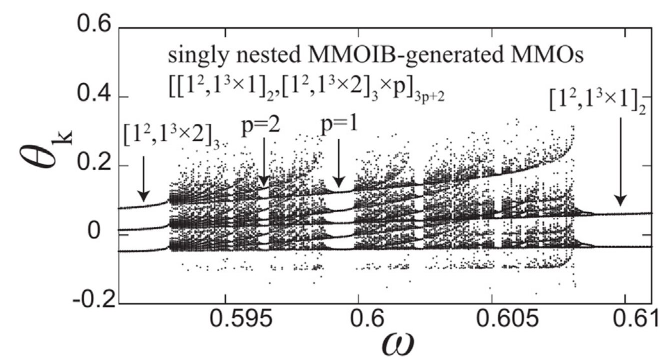

Fig. 9. Magnified view of one-parameter bifurcation diagram between $[1^2, 1^3 \times 1]_2$- and $[1^2, 1^3 \times 2]_3$-generating regions.

Our numerical results suggest that, in general, singly nested MMOIBs generate $[[1^s, 1^{s+1} \times m]_{m+1}, [1^s, 1^{s+1} \times (m+1)]_{m+2} \times p]_{(m+2)p+(m+1)}$ for successive p and integer values of s and m. The above-mentioned singly nested MMOs correspond to the $s = 2$ and $m = 1$ cases.

Figs. 10(a)–(f) show Poincaré return maps and the corresponding trajectories for singly nested MMOIB-generated $[[1^2, 1^3 \times 1]_2, [1^2, 1^3 \times 2]_3 \times p]_{3p+2}$ MMOs with $p = 1$–6. The singly nested MMOs could occur as many times as we track.

The singly nested $[A_1, B_1 \times p]$ MMOs could increment sequentially and terminate with $p \to \infty$ toward MMO incrementing-terminating tangent bifurcation point for T applied thrice (because the number of the forcing term (the final subscript) of $B_1 = [1^2, 1^3 \times 2]_3$ at which these singly nested MMOs accumulate is three). $T^3(\theta)$ at the tangent point for $[A_1, B_1 \times p]$ with $p \to \infty$ is shown in Fig. 11. The tangent bifurcation point for the singly nested MMO sequences can be obtained by solving the following

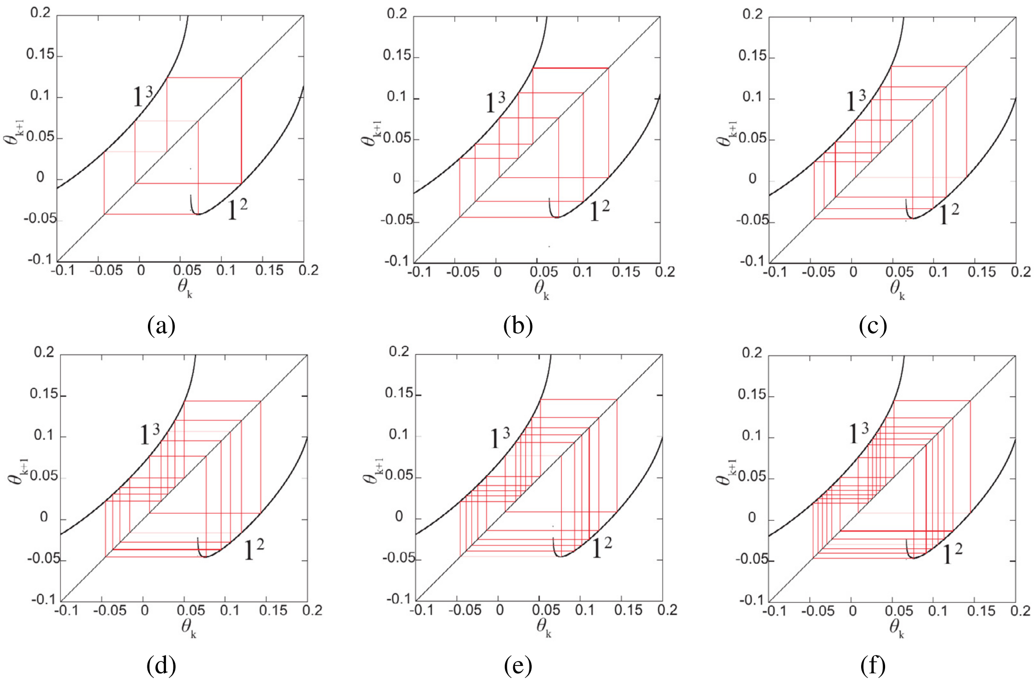

Fig. 10. 1D Poincaré return maps and corresponding trajectories of singly nested MMOIB-generated $[[1^2, 1^3 \times 1]_2, [1^2, 1^3 \times 2]_3 \times p]_{3p+2}$ MMOs, showing (a) $p = 1$ with $\omega = 0.5995$, (b) $p = 2$ with $\omega = 0.5966$, (c) $p = 3$ with $\omega = 0.59525$, (d) $p = 4$ with $\omega = 0.59459$, (e) $p = 5$ with $\omega = 0.59417$, and (f) $p = 6$ with $\omega = 0.59389$.

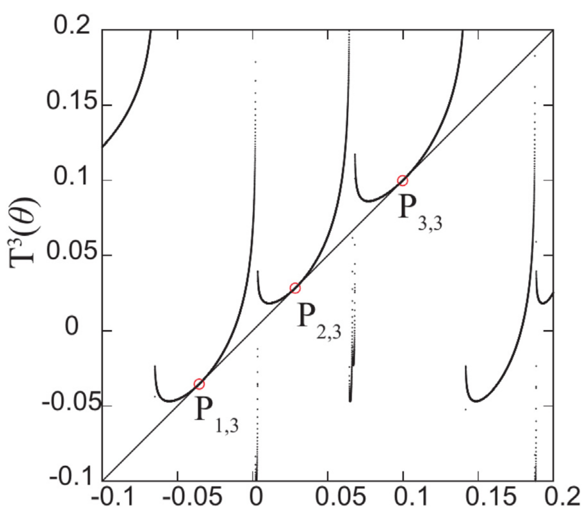

Fig. 11. $T^3(\theta)$ at MMO incrementing–terminating tangent bifurcation point for singly nested $[A_1, B_1 \times p]$ MMOs with $p \to \infty$ for $\omega = 0.592864855$.

simultaneous equations:

$$\begin{aligned} &T^3(\theta, \omega) = \theta, \\ &\frac{\partial}{\partial \theta} T^3(\theta, \omega) = 1. \end{aligned} \tag{11}$$

The successive generation of these singly nested MMOs is well explained by this map. $T(\theta)$ applied thrice is tangential to the diagonal line at three points, $P_{1,3}$, $P_{2,3}$, and $P_{3,3}$. $T(P_{1,3}) = P_{2,3}$, $T(P_{2,3}) = P_{3,3}$, and $T(P_{3,3}) = P_{1,3}$ hold at this tangent point.

Finally, we discuss doubly nested MMOs. Let two adjacent singly nested MMOs be denoted by $[A_1, B_1 \times 1] = [[1^2, 1^3 \times 1]_2, [1^2, 1^3 \times 2]_3 \times 1]_5 \equiv A_2$ and $[A_1, B_1 \times 2] = [[1^2, 1^3 \times 1]_2, [1^2, 1^3 \times 2]_3 \times 2]_8 \equiv B_2$. Between the A_2- and B_2-generating regions, doubly nested MMOIB-generated MMOs produce sequences represented by $[A_2, B_2 \times q] = [[[1^2, 1^3 \times 1]_2, [1^2, 1^3 \times 2]_3 \times 1]_5, [[1^2, 1^3 \times 1]_2, [1^2, 1^3 \times 2]_3 \times 2]_8 \times q]_{8q+5}$ sequentially with successive values of q. A highly magnified view of a one-parameter bifurcation diagram is shown in Fig. 12. Since the doubly nested MMO sequences are very long, they appear in small intervals of the bifurcation parameter ω. However, they could be observed as many times as we track. The doubly nested MMO attractors for $q = 1$–6 are shown in Figs. 13(a)–(f), respectively. These phenomena could be almost indistinguishable just by observing the time series waveforms alone [51,52,54]. In addition, it is difficult to distinguish them even if we use 1D Poincaré return maps because the period of the sequence is already 53 when $q = 6$.

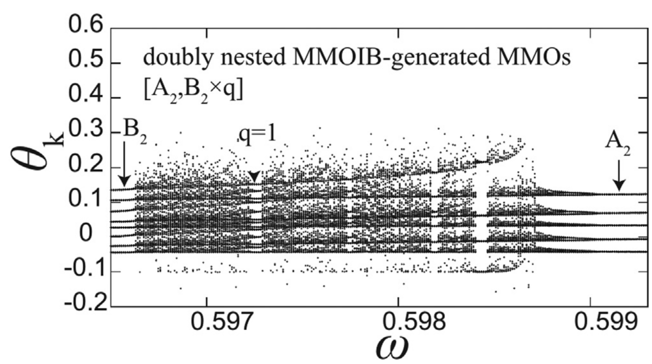

Fig. 12. Highly magnified view of one-parameter bifurcation diagram between the $A_2 = [[1^2, 1^3 \times 1]_2, [1^2, 1^3 \times 2]_3 \times 1]_5$- and $B_2 = [[1^2, 1^3 \times 1]_2, [1^2, 1^3 \times 2]_3 \times 2]_8$-generating regions where doubly nested MMOs can be observed.

The doubly nested $[A_2, B_2 \times q]$ MMOs could increment sequentially and terminate with $q \to \infty$ toward MMO incrementing–terminating tangent bifurcation point. Since the number of the forcing term (the final subscript) of B_2 is 8, T applied 8 times is tangential to the diagonal line at the tangent bifurcation point. T applied 8 times at the tangent point is shown in Fig. 14. The tangent bifurcation point for these doubly nested MMO sequences

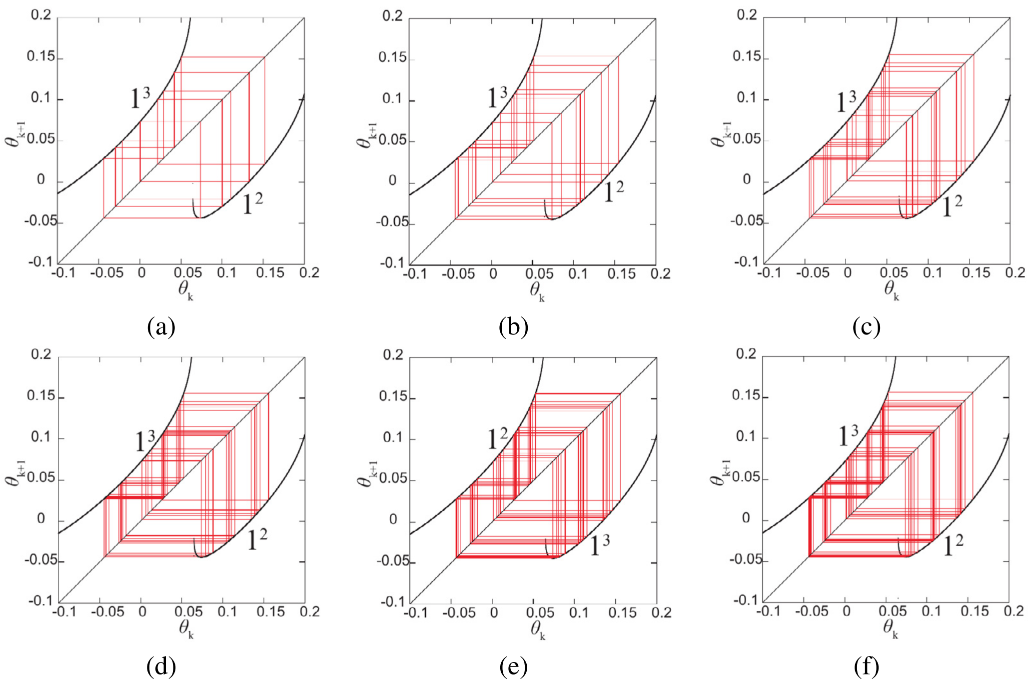

Fig. 13. 1D Poincaré return maps and corresponding trajectories of doubly nested MMOIB-generated $[[[1^2, 1^3 \times 1]_2, [1^2, 1^3 \times 2]_3 \times 1]_5, [[1^2, 1^3 \times 1]_2, [1^2, 1^3 \times 2]_3 \times 2]_8 \times q]_{8q+5}$ MMOs, showing (a) $q = 1$ with $\omega = 0.59728$, (b) $q = 2$ with $\omega = 0596903$, (c) $q = 3$ with $\omega = 0.597765$, (d) $p = 4$ with $\omega = 0.5967192$, (e) $p = 5$ with $\omega = 0.59668805$, and (f) $p = 6$ with $\omega = 0.59666905$.

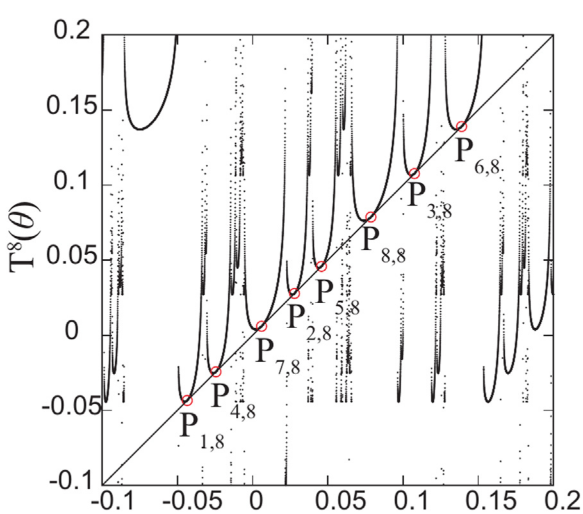

Fig. 14. $T^8(\theta)$ at MMO incrementing–terminating tangent bifurcation point for doubly nested $[A_2, B_2 \times q]$ MMOs with $q \to \infty$ for $\omega = 0.592864855$.

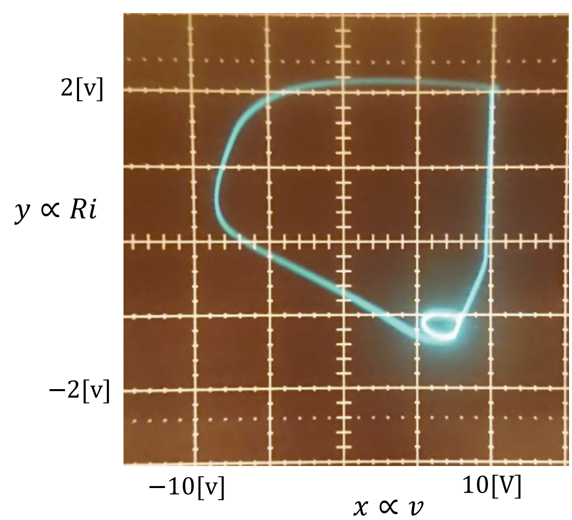

Fig. 15. 1^2 attractor in x–y plane for $f = 1,200$ Hz.

can be obtained by solving the following simultaneous equations numerically:

$$
\begin{aligned}
&T^8(\theta, \omega) = \theta, \\
&\frac{\partial}{\partial \theta} T^8(\theta, \omega) = 1.
\end{aligned} \tag{12}
$$

Our numerical results suggest that doubly nested MMOIBs could generate $[[[1^s, 1^{s+1} \times m]_{m+1}, [1^s, 1^{s+1} \times (m+1)]_{m+2} \times p]_{(m+2)p+(m+1)}$, $[[1^s, 1^{s+1} \times m]_{m+1}, [1^s, 1^{s+1} \times (m+1)]_{m+2} \times (p+1)]_{(m+2)(p+1)+(m+1)} \times q]_{(m+2)(p+1)q+(m+1)q+(m+2)p+(m+1)}$ between the $[[1^s, 1^{s+1} \times m]_{m+1}$, $[1^s, 1^{s+1} \times (m+1)]_{m+2} \times p]_{(m+2)p+(m+1)}$- and $[[1^s, 1^{s+1} \times m]_{m+1}$, $[1^s, 1^{s+1} \times (m+1)]_{m+2} \times (p+1)]_{(m+2)(p+1)+(m+1)}$-generating regions for integer values of s, m, and p and successive q. The above-mentioned numerical results correspond to the $s = 2, m = 1$, and $p = 1$ cases. In the figure, the relationships $P_{k+1,8} = T(P_{k,8})$ for $k = 1$–7 and $P_{1,8} = T(P_{8,8})$ are satisfied.

4. Circuit experiments for un-nested and nested MMOs

In this section, we conduct laboratory measurements and observe un-nested and nested MMOIB-generated MMOs. In addition, we realize circuit equipment for observing Poincaré return maps experimentally.

We set $L = 200$ mH, $C = 10$ nF, $R = 400$ Ω, $E_0 = 5.0$ V, $E_1 = 100$ mV, and $V = 10$ V and realized $g_1 = 5.0 \times 10^{-4}$ A/V and $g_3 = 5.0 \times 10^{-6}$ A^3/V using an element that included some diodes. We varied f as the bifurcation parameter.

Fig. 15 shows an experimentally realized 1^2 attractor in the x–y plane, which was constrained to $V = 10$ V when the diode

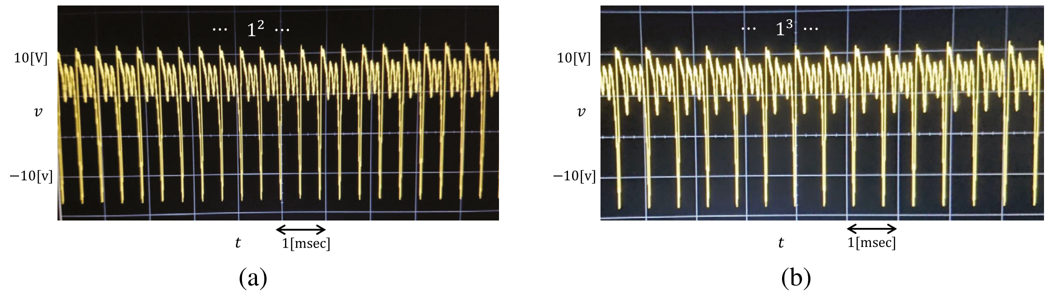

Fig. 16. Time series waveforms, showing (a) 1^2 for $f = 1,200$ Hz and (b) 1^3 for $f = 860$ Hz.

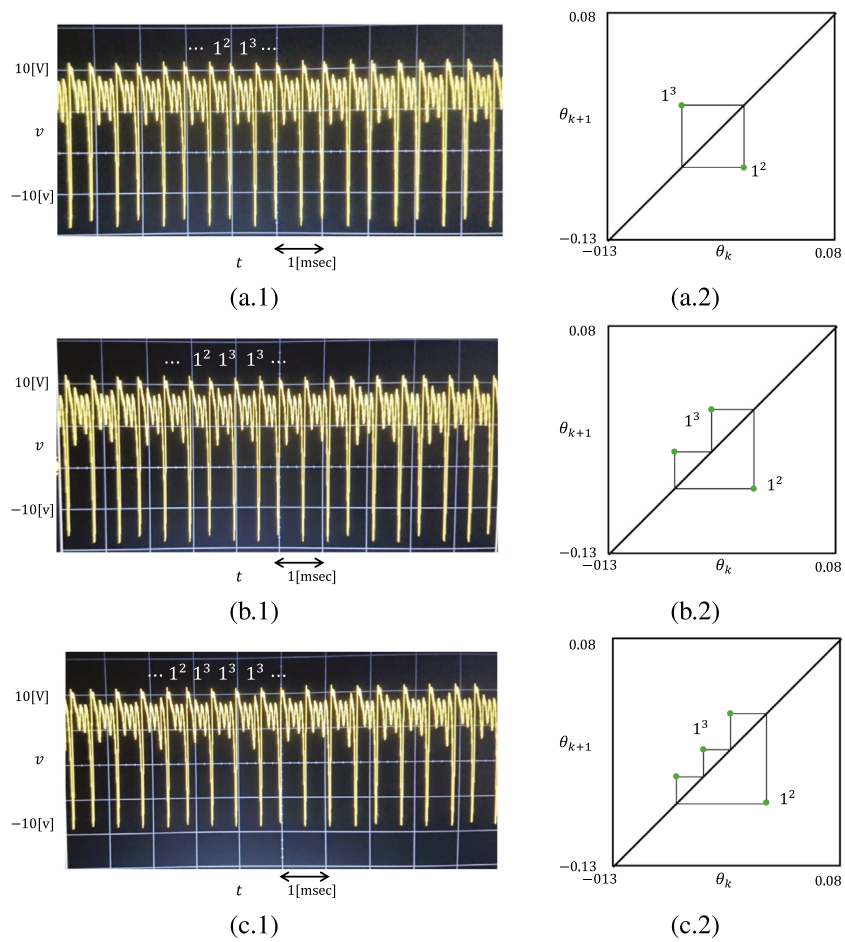

Fig. 17. (1) Time series waveforms and (2) corresponding Poincaré return maps, showing (a) $[1^2, 1^3 \times 1]_2$ for $f = 980$ Hz, (b) $[1^2, 1^3 \times 2]_3$ for $f = 946$ Hz, and (c) $[1^2, 1^3 \times 3]_4$ for $f = 922$ Hz.

was in the ON state and agrees with the numerically obtained solution shown in Fig. 4(a.2).

Figs. 16(a) and (b) show time series waveforms of simple 1^2 and 1^3 MMOs, which agrees with the numerically obtained ones shown in Figs. 4(a.1) and (e), respectively.

Figs. 17(a.1)–(c.1) and (a.2)–(c.2) show time series waveforms and the corresponding Poincaré return maps for un-nested MMOIB-generated $[1^2, 1^3 \times 1]_2$, $[1^2, 1^3 \times 2]_3$, and $[1^2, 1^3 \times 3]_4$ MMOs, respectively, obtained experimentally, which agrees with the numerical results shown in Figs. 4(b)–(d) and Figs. 7(a)–(c), respectively.

Finally, Figs. 18(1) and (2) show time series waveforms and the corresponding Poincaré return maps of singly nested $[[1^2, 1^3 \times 1]_2, [1^2, 1^3 \times 2]_3 \times 1]_5$ MMOs obtained experimentally, which were observed between the $[1^2, 1^3 \times 1]_2$- and $[1^2, 1^3 \times 2]_3$-generating regions and agrees with the numerical results shown in Fig. 10(a). We successfully observed simple, un-nested, and nested MMOs in the experimental measurements.

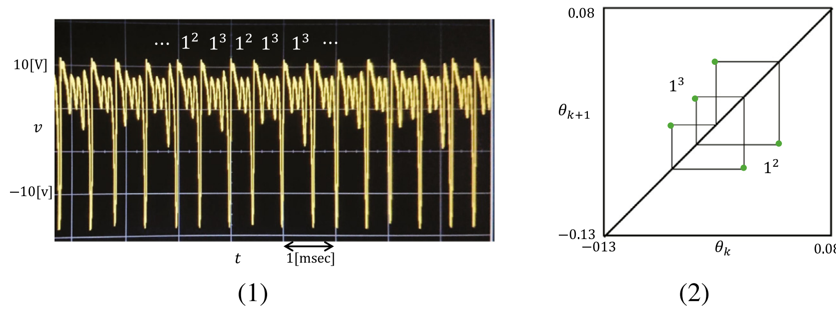

Fig. 18. (1) Time series waveforms and (2) corresponding Poincaré return maps of singly nested MMOs obtained experimentally, showing $[[1^2, 1^3 \times 1]_2, [1^2, 1^3 \times 2]_3 \times 1]_5$ for $f = 954$ Hz.

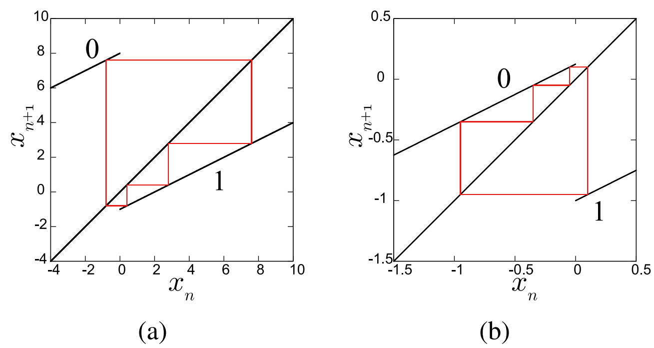

Fig. 19. Behavior of solutions caused by period-adding bifurcations. (a) "0111" for $a = 8$ and $b = 1$ and (b) "1000" for $a = 0.125$ and $b = 1$.

5. Nagumo–Sato piecewise-linear discontinuous 1D map

5.1. Introduction of Nagumo–Sato piecewise-linear discontinuous 1D map

In this section, we precisely review a 1D map proposed by Nagumo and Sato [60,66–68]. It is given by the following two-segment piecewise-linear discontinuous 1D map:

$$x_n = T(x_n) = \begin{cases} T_1(x_n) = \lambda_1 x_n + a & \text{if } x_n < 0, \\ T_2(x_n) = \lambda_2 x_n - b & \text{if } x_n > 0, \end{cases} \tag{13}$$

where $a > 0$, $b > 0$, $0 < \lambda_1 < 1$, and $0 < \lambda_2 < 1$ are assumed, and where $\Delta_1 = a/b$ is selected as the bifurcation parameter. We call Eq. (13) the Nagumo–Sato map. The dynamics always generate periodic solutions because the gradient of the map is less than unity for any $x_n \in R$. Since the Nagumo–Sato map is piecewise-linear, all solutions and parameter conditions are explicit. See Refs. [60–69] for more details on the Cantor function and a devil's staircase. Brief commentary on the $0 < \lambda_1 < 1$ and $0 < \lambda_2 < 1$ cases can be found in [69].

We focus on periodic solutions generated by the Nagumo–Sato map. Using T_1 and T_2, $T^4(x)$ can be written as $T_2(T_2(T_2(T_1(x))))$ if $x < 0$, $T_1(x) > 0$, $T_2(T_1(x)) > 0$, and $T_2(T_2(T_1(x))) > 0$. This can be written using the notation $T_2^3T_1$.

Fix $b = 1$. Then, $\Delta_1 = a$ is the bifurcation parameter. If a is larger and smaller, period-adding sequences are generated sequentially. It is assumed that 0 is output when the solution strikes branch T_1 and that 1 is output when the solution strikes branch T_2. The solution is uniquely determined by the output sequences of the symbolic dynamics.

The attractors in Figs. 19(a) and (b) are identified by the output sequences "0111" and "1000", respectively.

Note that $T_2^pT_1^q$ does not exist for $p \geq 2$ and $q \geq 2$. We prove this as follows. In order for the solution to output successive multiple 0s, $T_1(-b)$ must be less than 0. In order for the solution to output multiple 1s, $T(a)$ must be larger than 0. Therefore,

$$-\lambda_1 b + a < 0,\ \lambda_2 a - b > 0. \tag{14}$$

Thereby, $\lambda_1\lambda_2 > 1$ must be satisfied. However, this is contrary to the assumption.

5.2. Analysis of un-nested period-adding bifurcations of $T_2^mT_1$ and $T_1^mT_2$ types for successive m ($m \geq 1$)

In this section, we consider un-nested period-adding bifurcations, one of which corresponds to un-nested MMOIBs. First, we consider the case in which $T_2^mT_1$ ($m \geq 1$) has a stable fixed point. In this case, un-nested period-adding bifurcations 1^m0 are generated for successive m. When considering that the symbols are cyclic, symbolic sequence 1^m0 can be identified as 01^m, so, we write $1^m0 = 01^m$. $T_2^mT_1$ is written as

$$T_2^mT_1(x) = \lambda_1\lambda_2^m x + \lambda_2^m a - \frac{b(1-\lambda_2^m)}{1-\lambda_2}. \tag{15}$$

Let the fixed point of $T_2^mT_1(x)$ be denoted by $\bar{x}$. From $T_2^mT_1(\bar{x}) = \bar{x}$, $\bar{x}$ can be derived as

$$\bar{x} = \frac{\lambda_2^m a - \dfrac{b(1-\lambda_2^m)}{1-\lambda_2}}{1-\lambda_1\lambda_2^m}. \tag{16}$$

In order for $\bar{x}$ to be a fixed point, $-b < \bar{x} < 0$ must be satisfied. By solving this, the parameter condition that generates $\bar{x}$ is expressed as

$$\lambda_1 + \frac{1-\lambda_2^{m-1}}{\lambda_2^{m-1}(1-\lambda_2)} < \Delta_1 < \frac{1-\lambda_2^m}{\lambda_2^m(1-\lambda_2)}. \tag{17}$$

Similarly, we derive a condition in which $T_1^mT_2$ ($m \geq 1$) has a fixed point. In this case, un-nested period-adding bifurcations $0^m1 = 10^m$ are generated for successive m. $T_1^mT_2(x)$ is derived as follows.

$$T_1^mT_2(x) = \lambda_2\lambda_1^m x - \lambda_1^m b + a\frac{1-\lambda_1^m}{1-\lambda_1}. \tag{18}$$

Let the fixed point of $T_1^mT_2(x)$ be denoted by $\bar{\bar{x}}$. From $T_1^mT_2(\bar{\bar{x}}) = \bar{\bar{x}}$, $\bar{\bar{x}}$ can be given by

$$\bar{\bar{x}} = \frac{-\lambda_1^m b + a\dfrac{1-\lambda_1^m}{1-\lambda_1}}{1-\lambda_2\lambda_1^m}, \tag{19}$$

and such $\bar{\bar{x}}$ ($0 < \bar{\bar{x}} < a$) exists if

$$\lambda_2 + \frac{1-\lambda_1^{m-1}}{\lambda_1^{m-1}(1-\lambda_1)} < \frac{1}{\Delta_1} < \frac{1-\lambda_1^m}{\lambda_1^m(1-\lambda_1)}. \tag{20}$$

At first glance, un-nested period-adding bifurcations $T_1^mT_2$ and $T_1T_2^m$ appear to be similar to un-nested MMOIBs. However, only $[1^2, 1^3\times m]_{m+1}$ can be generated sequentially for successive m and the mirror sequence $[1^2\times m, 1^3]_{m+1}$ cannot emerge in the driven BVP oscillator because only branch 1^3 can be tangent to the diagonal line, but branch 1^2 can never be tangent to the diagonal line, as shown in Fig. 8. This is the main difference in the bifurcation structures between the Nagumo–Sato map and driven BVP oscillator. Namely, one of two un-nested period-adding bifurcations generated with the Nagumo–Sato map explains un-nested MMOIBs.

Note that the parameter interval of Eq. (20) for $m = 1$ coincides with that of Eq. (17) for $m = 1$. Note also that there are gaps between the parameter intervals, i.e., there are intervals of Δ_1 that satisfy the following equation:

$$\frac{1-\lambda_2^m}{\lambda_2^m(1-\lambda_2)} < \Delta_1 < \lambda_1 + \frac{1-\lambda_2^m}{\lambda_2^m(1-\lambda_2)}, \quad m = 1,2,3\cdots, \tag{21}$$

$$\frac{1-\lambda_1^m}{\lambda_1^m(1-\lambda_1)} < \frac{1}{\Delta_1} < \lambda_2 + \frac{1-\lambda_1^m}{\lambda_1^m(1-\lambda_1)}, \quad m = 1,2,3\cdots. \tag{22}$$

5.3. Analysis for nested period-adding bifurcations of $(T_2^{m+1}T_1)^p(T_2^mT_1)$ and $(T_2^{m+1}T_1)(T_2^mT_1)^p$ ($m\ge 1$) types for successive p ($p \ge 1$)

We analyze what phenomena are observed in the parameter gaps given by Eq. (21). From Eq. (17), these parameter gaps are regions between the intervals where $T_2^mT_1$ and $T_2^{m+1}T_1$ have a stable fixed point. In these regions,

$$(T_2^{m+1}T_1)^p(T_2^mT_1) \text{ for } p\ge 1, \tag{23}$$

and

$$(T_2^{m+1}T_1)(T_2^mT_1)^p \text{ for } p\ge 1, \tag{24}$$

have a stable fixed point where m is a fixed integer, and singly nested period-adding bifurcations

$$(1^{m+1}0)^p(1^m0) = (01^m)(01^{m+1})^p \text{ for } p\ge 1, \tag{25}$$

and

$$(1^{m+1}0)(1^m0)^p = (01^m)^p(01^{m+1}) \text{ for } p\ge 1, \tag{26}$$

can occur, which are among the four possible singly nested period-adding bifurcations.

To analyze nested period-adding bifurcations, let us consider the following composite map:

$$\Pi_1(x) = T_2^mT_1(x). \tag{27}$$

Solving $\Pi(x^\top) = 0$ yields

$$x^\top = -\frac{a}{\lambda_1} + \frac{b(1-\lambda_2^m)}{\lambda_1\lambda_2^m(1-\lambda_2)}. \tag{28}$$

Therefore, $\Pi_1(x)$ on the interval $-b \le x < 0$ is represented by

$$\Pi_1(x) = \begin{cases} \lambda_1\lambda_2^m x + \lambda_2^m a - \dfrac{b(1-\lambda_2^m)}{1-\lambda_2} & \text{for } -b\le x < x^\top, \\ \lambda_1\lambda_2^{m+1}x + \lambda_2^{m+1}a - \dfrac{b(1-\lambda_2^{m+1})}{1-\lambda_2} & \text{for } x^\top < x < 0. \end{cases} \tag{29}$$

Via the transformation of $y = x - x^\top$ and $\Pi = \Pi_1 - x^\top$, $\Pi(y)$ is represented as

$$\Pi(y) = \begin{cases} \lambda_1\lambda_2^m y + \frac{1}{\lambda_1\lambda_2^m}\left(\lambda_2^m a - \dfrac{b(1-\lambda_2^m)}{1-\lambda_2}\right) & \text{for } y<0, \\ \lambda_1\lambda_2^{m+1}y - b + \frac{1}{\lambda_1\lambda_2^m}\left(\lambda_2^m a - \dfrac{b(1-\lambda_2^m)}{1-\lambda_2}\right) & \text{for } y>0. \end{cases} \tag{30}$$

Thus, Π is written by the following form.

$$y_{n+1} = \Pi(y_n) = \begin{cases} \lambda_1^1 y_n + a^1, & \text{for } y_n < 0, \\ \lambda_2^1 y_n - b^1, & \text{for } y_n > 0, \end{cases} \tag{31}$$

where

$$\begin{aligned} &\lambda_1^1 = \lambda_1\lambda_2^m,\ \lambda_2^1 = \lambda_1\lambda_2^{m+1}, \\ &a^1 = \frac{1}{\lambda_1\lambda_2^m}\left(\lambda_2^m a - b\frac{1-\lambda_2^m}{1-\lambda_2}\right), \\ &b^1 = b - \frac{1}{\lambda_1\lambda_2^m}\left(\lambda_2^m a - b\frac{1-\lambda_2^m}{1-\lambda_2}\right). \end{aligned} \tag{32}$$

Note that Π in Eq. (31) has the same form as T in Eq. (13). Therefore, the period-adding bifurcations can be nested. Furthermore, by considering the similar discussions for the nested map of Eq. (31), it can be understood easily that the bifurcation structures of period-adding bifurcations can be nested as many times as desired.

By applying Eqs. (17) and (20) to Eq. (31), one of the four singly nested maps $(T_2^{m+1}T_1)^p(T_2^mT_1)$ has a stable fixed point if

$$\lambda_1^1 + \frac{1-(\lambda_2^1)^{p-1}}{(\lambda_2^1)^{p-1}(1-\lambda_2^1)} < \Delta_2 < \frac{1-(\lambda_2^1)^p}{(\lambda_2^1)^p(1-\lambda_2^1)}, \tag{33}$$

and $(T_2^{m+1}T_1)(T_2^mT_1)^p$ has a stable fixed point if

$$\lambda_2^1 + \frac{1-(\lambda_1^1)^{p-1}}{(\lambda_1^1)^{p-1}(1-\lambda_1^1)} < \frac{1}{\Delta_2} < \frac{1-(\lambda_1^1)^p}{(\lambda_1^1)^p(1-\lambda_1^1)}, \tag{34}$$

where $\Delta_2 = a^1/b^1$. Note that Eq. (33) coincides with Eq. (34) if $p = 1$. The existence of fixed points of $(T_2^{m+1}T_1)^p(T_2^mT_1)$ and $(T_2^{m+1}T_1)(T_2^mT_1)^p$ indicate that the following sequences exist:

$$(1^{m+1}0)^p(1^m0) = (01^m)(01^{m+1})^p \text{ for } p\ge 1, \tag{35}$$

and

$$(1^{m+1}0)(1^m0)^p = (01^{m+1})(01^m)^p \text{ for } p\ge 1, \tag{36}$$

which are among four possible singly nested period-adding bifurcations.

By conducting similar discussions for

$$\Pi_2(x) = T_1^mT_2(x), \tag{37}$$

the existence of the fixed point for the other singly nested maps $(T_1^mT_2)^p(T_1^{m+1}T_2)$ and $(T_1^{m+1}T_2)^p(T_1^mT_2)$ can be proven. They indicate that the following sequences exist:

$$(0^m1)^p(0^{m+1}1), \text{ for } p\ge 1, \tag{38}$$

and

$$(0^{m+1}1)^p(0^m1), \text{ for } p\ge 1, \tag{39}$$

which are among the four possible singly nested period-adding bifurcations.

Eqs. (35), (36), (38), and (39) represent the four possible singly nested period-adding bifurcations.

5.4. Relationship for nested solutions generated between driven BVP oscillator and Nagumo–Sato map

To consider the relationship for the nested solutions generated between the driven BVP oscillator discussed in this study and the Nagumo–Sato map, make 1^3 correspond to 0 and 1^2 to 1 where the $s = 2$ case is considered. It is shown in this paper that one of the possible solutions of un-nested, singly and doubly nested period-adding bifurcations generated by the Nagumo–Sato map coincide with un-nested, singly and doubly nested MMOIBs in the BVP oscillator.

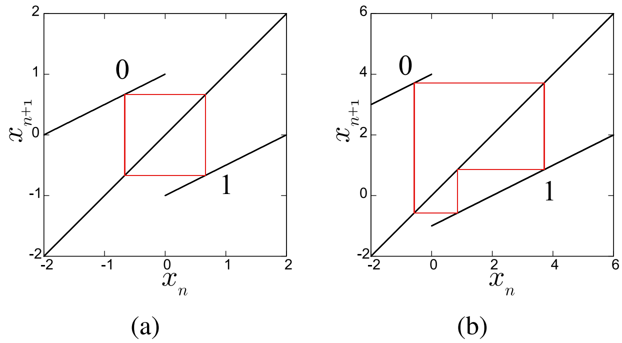

Fig. 20. Behavior of solutions caused by un-nested period-adding bifurcations, showing (a) "01" for $a = 1$ and $b = 1$ and (b) "011" for $a = 4$ and $b = 1$.

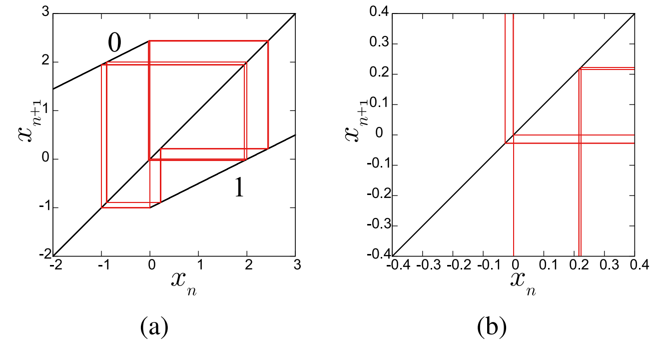

Fig. 22. Behavior of solution caused by doubly nested bifurcation, showing (a) "0101101011011" for $a = 2.445$ and $b = 1$ and (b) a magnified view of (a).

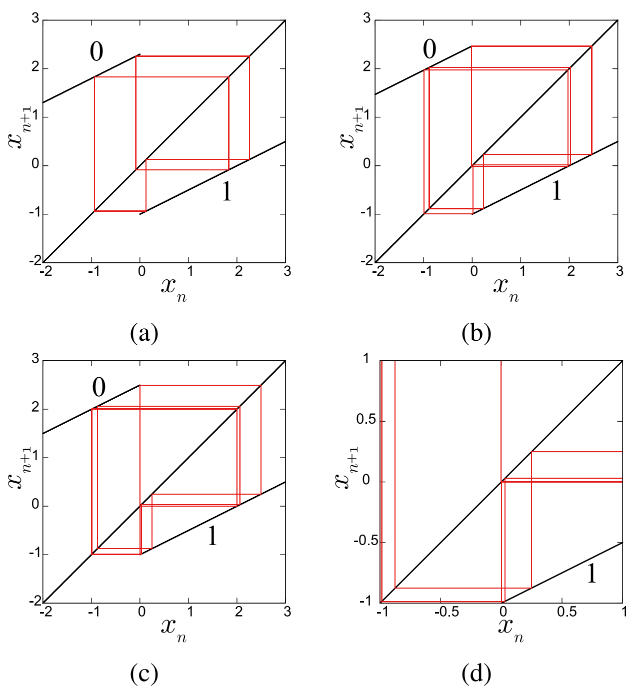

Fig. 21. Behavior of solutions caused by singly nested period-adding bifurcations, showing (a) "01011" for $a = 2.3$ and $b = 1$, (b) $01(011)^2$ for $a = 2.47$ and $b = 1$, (c) $01(011)^3$ for $a = 2.497$ and $b = 1$, and (d) magnified view of (c).

For the un-nested case, MMOIBs that correspond to period-adding bifurcations for maps represented by $1^m0 = 01^m$ can occur sequentially for successive m, but MMOIBs represented by $0^m1 = 10^m$ cannot do so because both branches in the invariant interval of the Poincaré return map T are downward convex. Figs. 7(a)–(d) show $m = 1, 2, 3$, and 10 cases for the driven BVP oscillator. Figs. 20(a) and (b) and 19(a) show trajectories of the Nagumo–Sato map for $m = 1, 2$, and 3, respectively.

For the same reason, singly nested MMOIBs $(01^m)(01^{m+1})^p$ can occur for successive p, which is one of the four possible singly nested period-adding bifurcations (Eqs. (35), (36), (38), and (39)) generated by the Nagumo–Sato map. Figs. 21(a), (b), and (c) show the solution of Eq. (35) for the $m = 1$, and $p = 1, 2$, and 3 cases, respectively. Fig. 21(d) shows a magnified view of Fig. 21(c). Figs. 10(a)–(f) show the $m = 1$ and $p = 1, 2, 3, 4, 5$, and 6 cases for the driven BVP oscillator.

For the same reason, $((01^m)(01^{m+1})^p)((01^m)(01^{m+1})^{p+1})^q$ can occur for integer values of m and p and successive q between the $(01^m)(01^{m+1})^p$- and $(01^m)(01^{m+1})^{p+1}$-generating regions, which is among the eight possible cases for doubly nested period-adding bifurcations generated by the Nagumo–Sato map. Figs. 22(a) and (b) show the attractor and a magnified view for the $m = p = q = 1$ cases. Figs. 13(a)–(f) correspond to the $m = p = 1$ and $q = 1$–6 cases, respectively, for the driven BVP oscillator.

The period-adding bifurcation structures generated by the Nagumo–Sato map suggest that more deeply nested MMOIBs exist in the driven BVP oscillator.

6. Conclusion

We analyzed a driven Bonhoeffer–van der Pol oscillator where the diode in the circuit was assumed to be an ideal switch. In this case, Poincaré return maps can be derived exactly as 1D and mixed-mode oscillation-incrementing bifurcations that are nested at least twice are precisely explained. In addition, the return maps are downward convex in the invariant interval. We considered a piecewise linear discontinuous approximation for the return map in the invariant interval. The piecewise linear map is called the Nagumo–Sato map, generating infinitely many nested period-adding bifurcations. We confirmed that un-nested, singly and doubly nested mixed-mode oscillation-incrementing bifurcations in the driven BVP oscillator coincide with one of the possible period-adding solutions generated by the Nagumo–Sato map because mirror sequences do not exist in the driven BVP oscillator.

CRediT authorship contribution statement

Naohiko Inaba: Supervision, Writing – original draft, Conceptualization, Methodology, Software. **Tadashi Tsubone:** Validation, Investigation. **Hidetaka Ito:** Project administration, Data curation, Formal analysis, Writing – review & editing. **Hideaki Okazaki:** Validation, Investigation, Resources. **Tetsuya Yoshinaga:** Investigation, Funding acquisition.

Declaration of competing interest

The authors declare that they have no known competing financial interests or personal relationships that could have appeared to influence the work reported in this paper.

Data availability

Data will be made available on request.

Acknowledgments

This work was supported by JSPS, Japan KAKENHI Grant Number 21K04080.

References

[1] M. Diener, The canard unchained or how fast/slow dynamical systems bifurcate, Math. Intelligencer 6 (1984) 38–49.
[2] A.K. Zvonkin, M.A. Shubin, Non-standard analysis and singular perturbations of ordinary differential equations, Russian Math. Surveys 39 (1984) 69–131.
[3] S.M. Baer, T. Erneux, Singular Hopf bifurcation to relaxation oscillations, SIAM J. Appl. Math. 46 (1986) 721–739.
[4] S.M. Baer, T. Erneux, Singular Hopf bifurcation to relaxation oscillations. II, SIAM J. Appl. Math. 52 (1992) 1651–1664.
[5] B. Braaksma, J. Grasman, Critical dynamics of the Bonhoeffer-van der Pol equation and its chaotic response to periodic stimulation, Physica D 68 (1993) 265–280.
[6] V.I. Arnol'd (Ed.), Encyclopedia of Mathematical Sciences 5, Springer–Verlag, 1994.
[7] J. Guckenheimer, K. Hoffman, W. Weckesser, Numerical computation of canards, Int. J. Bifurc. Chaos 10 (2000) 2669–2687.
[8] J.L. Hudson, M. Hart, D. Marinko, An experimental study of multiple peak periodic and nonperiodic oscillations in the Belousov–Zhabotinskii reaction, J. Chem. Phys. 71 (1979) 1601–1606.
[9] M. Orban, I.R. Epstein, Complex periodic and aperiodic oscillation in the chlorite-thiosulfate reaction, J. Phys. Chem. 86 (1982) 3907–3910.
[10] J. Maselko, H.L. Swinney, Complex periodic oscillations and Farey arithmetic in the Belousov–Zhabotinskii reaction, J. Chem. Phys. 85 (1986) 6430–6441.
[11] F.N. Albahadily, J. Ringland, M. Schell, Mixed-mode oscillations in an electrochemical system. I. A Farey sequence which does not occur on a torus, J. Chem. Phys. 90 (1989) 813–821.
[12] M. Brøns, T.J. Kaper, H.G. Rotstein, Introduction to focus issue: Mixed mode oscillations: experiment, computation, and analysis, Chaos 18 (2008) 015101.
[13] V. Petrov, S.K. Scott, K. Showalter, Mixed-mode oscillations in chemical systems, J. Chem. Phys. 97 (1992) 6191–6198.
[14] T. Yoshinaga, H. Kawakami, K. Yoshikawa, A circuit metaphor for nonlinear oscillation in a chemical system at a water-oil interface, IEICE Trans. J71-A (1988) 1843–1851 (in Japanese).
[15] C. Kuehn, Multiple Time Scale Dynamics, Springer International Publishing, 2015.
[16] S.K. Scott, Chemical Chaos, Oxford University Press, 1993.
[17] M. Brøns, M. Krupa, M. Wechselberger, Mixed mode oscillations due to the generalized canard phenomenon, Fields Inst. Commun. 49 (2006) 39–63.
[18] M. Krupa, N. Popović, N. Kopel, Mixed-mode oscillations in three time-scale systems: A prototypical example, SIAM J. Appl. Dyn. Syst. 7 (2008) 361–420.
[19] M. Krupa, M. Wechselberger, Local analysis near a folded saddle–node singularity, J. Differ. Equ. 248 (2010) 2841–2888.
[20] G. Markman, K. Bar-Eli, Periodic perturbations of an oscillatory chemical system, J. Phys. Chem. 98 (1994) 12248–12254.
[21] M. Brøns, P. Gross, K. Bar-Eli, Circle maps and the devil's staircase in a periodically perturbed oregonator, Int. J. Bifurc. Chaos 11 (1997) 2621–2628.
[22] A.L. Kawczyński, V.O. Khavrus, P.E. Strizhak, Complex mixed-mode periodic and chaotic oscillations in a simple three-variable model of nonlinear system, Chaos 10 (2000) 299–310.
[23] A.L. Kawczyński, P.E. Strizhak, Period adding and broken Farey tree sequence of bifurcations for mixed-mode oscillations and chaos in the simplest three-variable nonlinear system, J. Chem. Phys. 112 (2000) 6122–6130.
[24] M. Sekikawa, N. Inaba, T. Yoshinaga, T. Hikihara, Period-doubling cascades of canards from the extended Bonhoeffer-van der Pol oscillator, Phys. Lett. A 374 (2010) 3745–3751.
[25] K. Shimizu, M. Sekikawa, N. Inaba, Mixed-mode oscillations and chaos from a simple second-order oscillator under weak periodic perturbation, Phys. Lett. A 375 (2011) 1566–1569.
[26] K. Shimizu, Y. Saito, M. Sekikawa, N. Inaba, Complex mixed-mode oscillations in a Bonhoeffer-van der Pol oscillator under weak periodic perturbation, Physica D 241 (2012) 1518–1526.
[27] K. Shimizu, M. Sekikawa, N. Inaba, Experimental study of complex mixed-mode oscillations generated in a Bonhoeffer-van der Pol oscillator under weak periodic perturbation, Chaos 25 (2015) 023105.
[28] K. Shimizu, N. Inaba, Piecewise-linear Bonhoeffer-van der Pol dynamics explaining mixed-mode oscillation-incrementing bifurcations, Prog. Theor. Exp. Phys. 2016 (2016) 033A01.
[29] K. Shimizu, N. Inaba, Experimental and numerical observation of successive mixed-mode oscillation-incrementing bifurcations in an extended Bonhoeffer-van der Pol oscillator, Int. J. Bifurc. Chaos 28 (2018) 1830047.
[30] E. Kutafina, Mixed mode oscillations in the Bonhoeffer-van der Pol oscillator with weak periodic perturbation, Comput. Appl. Math. 34 (2015) 81–92.
[31] P. De Maesschalck, E. Kutafina, N. Popović, Three time-scales in an extended Bonhoeffer-van der Pol oscillator, J. Dyn. Differ. Equ. 26 (2014) 955–987.
[32] J.G. Freire, J.A.C. Gallas, Stern–Brocot trees in the periodicity of mixed-mode oscillations, Phys. Chem. Chem. Phys. 13 (2011) 12191–12198.
[33] M. Desroches, T.J. Kaper, M. Krupa, Mixed-mode bursting oscillations: Dynamics created by a slow passage through spike-adding canard explosion in a square-wave burster, Chaos 23 (2013) 046106.
[34] J. Guckenheimer, C. Scheper, A geometric model for mixed-mode oscillations in a chemical system, SIAM J. Appl. Dyn. Syst. 10 (2011) 92–128.
[35] M. Desroches, J. Guckenheimer, B. Krauskopf, C. Kuehn, H.M. Osinga, M. Wechselberger, Mixed-mode oscillations with multiple time scales, SIAM Rev. 54 (2012) 211–288.
[36] J.G. Freire, J.A.C. Gallas, Stern–Brocot trees in cascades of mixed-mode oscillations and canards in the extended Bonhoeffer-van der Pol and the FitzHugh–Nagumo models of excitable systems, Phys. Lett. A 375 (2011) 1097–1103.
[37] L. Ryashko, Sensitivity analysis of the noise-induced oscillatory multistability in Higgins model of glycolysis, Chaos 28 (2018) 033602.
[38] C.B. Muratov, E. Vanden-Eijnden, Noise-induced mixed-mode oscillations in a relaxation oscillator near the onset of a limit cycle, Chaos 18 (2008) 015111.
[39] S. Sadhu, C. Kuehn, Stochastic mixed-mode oscillations in a three-species predator–prey model, Chaos 28 (2018) 033606.
[40] N.M. Awal, I.R. Epstein, Period-doubling route to mixed-mode chaos, Phys. Rev. E 104 (2021) 024211.
[41] S. Leo Kingston, K. Thamilmaran, Bursting oscillations and mixed-mode oscillations in driven Liénard system, Int. J. Bifurc. Chaos 7 (2017) 1730025.
[42] S.D. Vijay, S.L. Kingston, K. Thamilmaran, Different transitions of bursting and mixed-mode oscillations in Liénard system, Int. J. Electron. Commun. 111 (2019) 152898.
[43] M. Rachwalska, A.L. Kawczyński, Period-adding bifurcations in mixed-mode oscillations in the Belousov Zhabotinsky reactions at various residence times in a CSTR, J. Phys. Chem. 105 (2001) 7885–7888.
[44] G.M. Ngueuteu, R. Yamapi, P. Woafo, Quasi-static transient and mixed mode oscillations induced by fractional derivatives effect on the slow flow near folded singularity, Nonlinear Dynam. 78 (2014) 2717–2729.
[45] K. Tsumoto, Y. Kurata, K. Furutani, Y. Kurachi, Hysteretic dynamics of multi-stable early after depolarisations with repolarisation reserve attenuation: A potential dynamical mechanism for cardiac arrhythmias, Sci. Reps. 7 (2017) 10771.
[46] M. Sekikawa, T. Kousaka, T. Tsubone, N. Inaba, H. Okazaki, Bifurcation analysis of mixed-mode oscillations and Farey trees in an extended Bonhoeffer-van der Pol oscillator, Physica D 433 (2022) 133178.
[47] N. Inaba, T. Kousaka, T. Tsubone, H. Okazaki, H. Ito, Mixed-mode oscillations from a constrained extended Bonhoeffer-van der Pol oscillator with a diode, Chaos 31 (2021) 073133.
[48] M. Sekikawa, N. Inaba, Bifurcation structures of nested mixed-mode oscillation, Int. J. Bifurc. Chaos 31 (2021) 2150121.
[49] H. Takahashi, T. Kousaka, H. Asahara, N. Stankevich, N. Inaba, Mixed-mode oscillation-incrementing bifurcations and a devil's staircase from a nonautonomous constrained Bonhoeffer-Van Der Pol oscillator, Prog. Theor. Exp. Phys. 2018 (2018) 103A02.
[50] T. Kousaka, Y. Ogura, K. Shimizu, H. Asahara, N. Inaba, Analysis of mixed-mode oscillation-incrementing bifurcations generated in a nonautonomous constrained Bonhoeffer-van der Pol oscillator, Physica D 353–354 (2017) 48–57.
[51] N. Inaba, T. Tsubone, Nested mixed-mode oscillations, part II: Experimental and numerical study of a classical Bonhoeffer-van der Pol oscillator, Physica D 406 (2020) 132493.
[52] N. Inaba, T. Kousaka, Nested mixed-mode oscillations, Physica D 401 (2020) 132152.
[53] H. Ito, N. Inaba, H. Okazaki, Successive nested mixed-mode oscillations, NOLTA IEICE 12 (2021) 88–102.
[54] K. Kato, N. Inaba, K. Shimizu, T. Kousaka, H. Okazaki, Nested mixed-mode oscillations in a canard-generating driven Bonhoeffer-van der Pol oscillator, Physica D 440 (2022) 133438.
[55] R. FitzHugh, Impulses and physiological states in theoretical models of nerve membrane, Biophys. J. 1 (1961) 445–466.
[56] J. Nagumo, S. Animoto, S. Yoshizawa, An active pulse transmission line simulating nerve axon, Proc. Inst. Radio Eng. 50 (1962) 2061–2070.
[57] N. Inaba, T. Saito, S. Mori, Chaotic phenomena in a circuit with a negative resistance and an ideal switch of diode, IEICE Trans. E-70 (1987) 744–754.
[58] N. Inaba, S. Mori, Chaotic phenomena in a circuit with a diode due to the change of the oscillation frequency, IEICE Trans. E-71 (1988) 842–849.
[59] N. Inaba, S. Mori, Chaos via torus breakdown in a piecewise-linear forced van der Pol oscillator with a diode, IEEE Trans. Circuits Syst. 38 (1991) 398–409.
[60] J. Nagumo, S. Sato, On a response characteristic of a mathematical neuron model, Kybernetik 10 (1972) 155–164.

[61] S. Sato, Mathematical properties of responses of a neuron model: A system as a rational number generator, Kybernetik 11 (1972) 208–216.
[62] S. Sato, M. Hatta, J. Nagumo, Response characteristics of a neuron model to a periodic input, Kybernetik 16 (1974) 1–8.
[63] M. Hata, Dynamics of Caianiello's equation, J. Math. Kyoto Univ. 22 (1982) 155–173.
[64] T. Yoshida, On periodic responses of a mathematical neuron model, Biol. Cybernet. 52 (1985) 383–390.
[65] S. Doi, Response characteristics of nonlinear models to external stimuli: Neuron models and biological oscillators as an example, IEICE Fundam. Rev. 13 (2020) 187–196.
[66] N.N. Leonov, On a discontinuous piecewise-linear pointwise mapping of a line into itself, Radiofisica 3 (1960) 496–510 (in Russian).
[67] N.N. Leonov, On the theory of a discontinuous mapping of a line into itself, Radiofisica 3 (1960) 872–886 (in Russian).
[68] On a discontinuous pointwise mapping of a line into itself, Dokl. Akad. Nauk SSSR 143 (1962) 1038–1041 (in Russian).
[69] C. Mira, Chaotic Dynamics, World Scientific, Singapore, 1987.
[70] R. Szalai, H.M. Osinga, Arnol'd tongues arising from a grazing-sliding bifurcation, SIAM J. Appl. Dyn. Sys. 8 (2009) 1434–1461.
[71] R. Szalai, H.M. Osinga, Invariant polygons in systems with grazing-sliding, Chaos 18 (2008) 023121.
[72] Y. Yoshitake, A. Sueoka, H. Tamura, N. Shoji, Vibrations of nonlinear systems with discontinuities (Case of forced self-excited vibration accompanied by dry friction), Trans. Jpn. Soc. Mech. Eng. C 61 (1995) 768–774 (in Japanese).